Nonlinear Dynamics and Systems Theory, **23** (1) (2023) 46–57

Asymmetric Duffing Oscillator: Jump Manifold and Border Set

J. Kyzioł and A. Okniński *

Politechnika Świętokrzyska, Al. 1000–lecia PP 7, 25-314 Kielce, Poland

Received: October 24, 2022; Revised: December 22, 2022

Abstract: The jump phenomenon, present in the forced asymmetric Duffing oscillator, is studied using the known steady-state asymptotic solution. The main result consists in construction of a new mathematical object – a jump manifold – encoding global information about all possible jumps. The jump manifold is computed for the forced asymmetric Duffing oscillator, and several examples of jumps are calculated, showing the advantages of the method.

Keywords: *metamorphoses of amplitude-frequency curves; jump phenomenon.*

Mathematics Subject Classification (2010): 34C05, 34C25, 34E05, 37G35, 70K30.

1 Introduction

In this work, we study steady-state dynamics of the forced asymmetric Duffing oscillator governed by the equation

$$\ddot{y} + 2\zeta\dot{y} + \gamma y^3 = F_0 + F\cos(\Omega t), \tag{1}$$

which has a single equilibrium position and a corresponding one-well potential [1], where ζ, γ, F_0, F are parameters and Ω is the angular frequency of the periodic force. This dynamical system in particular and Duffing-type equations in general, which can be used to describe pendulums, vibration absorbers, beams, cables, micromechanical structures, and electrical circuits, have a long history [2]. The equation of motion (1) can describe several nonlinear phenomena such as various nonlinear resonances, symmetry breaking, chaotic dynamics, period-doubling route to chaos, multistability and fractal dependence on initial conditions, and jumps [1–6].

* Corresponding author: mailto:fizao@tu.kielce.pl

Our work aims to research the jump phenomenon using the implicit function machinery. Kovacic and Brennan described and investigated jumps for the system (1) in their interesting study [1]. Recently, Kalmár-Nagy and Balachandran [6] applied a differential condition to detect vertical tangents, characteristic of the jump phenomenon.

A standard approach to nonlinear equations of the form (1) is based on asymptotic methods [7, 8]. More exactly, in the case of Eq.(1), approximate nonlinear resonances 1 : 1 are computed in the form

$$y\left(t\right)=A_0+A_1\cos\left(\Omega t+\theta\right), \tag{2a}$$

$$f_i\left(A_0,\ A_1,\ \Omega;\ \underline{c}\right)=0, \quad i=1,2,3, \tag{2b}$$

where A_0, A_1 and Ω fulfill nonlinear implicit amplitude-frequency response algebraic equations (2b) and $\underline{c}=(\gamma,\ \zeta,\ F,\ F_0)$ [1, 5, 9].

We have proposed in our earlier papers an analysis of differential properties of solutions of the implicit amplitude-frequency response equations, see [10] and references therein. It turns out that bifurcations of dynamics, such as hysteresis and jump phenomenon, are related to the appearance/disappearance of branches of solutions, as well as more complicated bifurcations such as, for example, the creation/destruction of solutions follow from the changes of differential properties of solutions of the equations (2b), induced by a change of the parameters $\underline{c}$. Analytical methods, permitting the prediction of metamorphoses of solutions, are of great help in numerical simulation. Our formalism applies also to several models of coupled oscillators [11, 12], see also [13].

The novelty of this work consists in defining, in the differential geometry formulation, the jump manifold encoding global information about all possible jumps. Our formalism generalizes the differential condition of Kalmár-Nagy and Balachandran [6] for an arbitrary implicit amplitude-frequency response function.

In the next section, we describe the steady-state solution (2a) [1,5,9], given by implicit equations (2b). Working in the framework developed in our earlier papers, see [10] and references therein, we compute the jump manifold in Section 3 (see Eq.(9a) and Table 2) which contains information about all possible jumps – this is the main achievement of this work. In Section 4, we compare the analytical predictions with the numerical solutions of Eq.(1). We summarize our results in the last Section 5.

2 The Steady-State Solution

The steady-state solution of Eq.(1) of the form (2a) was computed in Refs. [1, 5, 9] with the following implicit amplitude-frequency response equations (2b):

$$-A_1\Omega^2+3\gamma A_0^2A_1+\frac{3}{4}\gamma A_1^3-F\cos\theta = 0, \tag{3a}$$

$$-2\zeta A_1\Omega-F\sin\theta = 0, \tag{3b}$$

$$\gamma A_0^3+\frac{3}{2}\gamma A_0A_1^2-F_0 = 0. \tag{3c}$$

Eliminating θ from Eqs.(3a), (3b), we get two implicit equations for $A_0,\ A_1$, and Ω:

$$A_1^2\left(-\Omega^2+3\gamma A_0^2+\frac{3}{4}\gamma A_1^2\right)^2+4\Omega^2\zeta^2A_1^2 = F^2, \tag{4a}$$

$$\gamma A_0^3+\frac{3}{2}\gamma A_1^2A_0-F_0 = 0. \tag{4b}$$

Computing A_1^2 from Eq.(4b) and substituting into (4a), we obtain finally one implicit equation for A_0, Ω:

$$f(\Omega, A_0; \gamma, \zeta, F, F_0) = \sum_{k=0}^{9} c_k A_0^k = 0, \tag{5}$$

where the coefficients c_k are given in Table 1.

Table 1: Coefficients c_k of the polynomial (5).

$c_9 = 25\gamma^3$	$c_4 = 16\Omega^2\gamma F_0$
$c_8 = 0$	$c_3 = -9\gamma F_0^2 + 6\gamma F^2$
$c_7 = -20\Omega^2\gamma^2$	$c_2 = -4F_0\Omega^4 - 16\zeta^2\Omega^2 F_0$
$c_6 = -15\gamma^2 F_0$	$c_1 = 4\Omega^2 F_0^2$
$c_5 = -15\gamma^2 F_0$	$c_0 = -F_0^3$

We can also obtain an implicit equation for A_1, Ω. We solve the cubic equation (4b) for A_0 computing the only one real root:

$$A_0 = -\frac{A_1^2}{2Y} + Y, \quad Y \equiv \sqrt[3]{\sqrt{\frac{1}{8}A_1^6 + \frac{1}{4\gamma^2}F_0^2} + \frac{1}{2\gamma}F_0}. \tag{6}$$

Two other roots are indeed complex since the discriminant of Eq.(4b), $D = -4p^3 - 27q^2$, $p = \frac{3}{2}A_1^2, q = -\frac{F_0}{\gamma}$, $\gamma \neq 0$, is negative.

Then we substitute A_0, Y from Eq.(6) into Eq.(4a), obtaining finally a complicated but useful implicit equation for A_1, Ω:

$$g(\Omega, A_1; \gamma, \zeta, F, F_0) = A_1^2\left(3\gamma A_0^2 + \tfrac{3}{4}\gamma A_1^2 - \Omega^2\right)^2 + 4\Omega^2\zeta^2 A_1^2 - F^2 = 0, \tag{7}$$

where A_0 and Y are defined in (6).

3 Jump Phenomenon

3.1 Jump conditions and jump manifold

Jump conditions in the implicit function setting read [10]

$$f(\Omega, A_0; \gamma, \zeta, F, F_0) = 0, \tag{8a}$$

$$\frac{\partial f(\Omega, A_0; \gamma, \zeta, F, F_0)}{\partial A_0} = 0, \tag{8b}$$

where equation (8b) is the condition for a vertical tangency.

Solving equations (8), we obtain

$$J(A_0; \gamma, \zeta, F, F_0) = \sum_{k=0}^{21} a_k A_0^k = 0, \tag{9a}$$

$$\Omega^2 = \frac{\left(-50\gamma^4\right)A_0^{12} + 95\gamma^3 F_0 A_0^9 + \left(6F^2\gamma^2 - 39\gamma^2 F_0^2\right)A_0^6 + \left(3F^2\gamma F_0 - 7\gamma F_0^3\right)A_0^3 + F_0^4}{2A_0\left(F_0 - 10\gamma A_0^3\right)\left(F_0 - \gamma A_0^3\right)^2}, \tag{9b}$$

the non-zero coefficients a_k of the polynomial $J(A_0)$ are given in Table 2.

The polynomial $J(A_0)$, complicated as it is, encodes global information about all possible jumps. We shall thus refer to equation (9a), which defines an implicit function

Table 2: Non-zero coefficients of polynomial (9a).

$a_{21} = 4000\gamma^7\zeta^2$	$a_9 = 3248\gamma^3\zeta^2F_0^4 - 72F^2\gamma^3\zeta^2F_0^2$
$a_{18} = -16\,000\gamma^6\zeta^2F_0$	$a_8 = 36F^4\gamma^3F_0 - 978F^2\gamma^3F_0^3$
$a_{17} = 600F^2\gamma^6$	$a_6 = 528\gamma^2\zeta^2F_0^5 - 240F^2\gamma^2\zeta^2F_0^3$
$a_{15} = 23\,880\gamma^5\zeta^2F_0^2 - 480F^2\gamma^5\zeta^2$	$a_5 = 9F^4\gamma^2F_0^2 + 138F^2\gamma^2F_0^4$
$a_{14} = -1920F^2\gamma^5F_0$	$a_3 = 24F^2\gamma\zeta^2F_0^4 - 152\gamma\zeta^2F_0^6$
$a_{12} = 768F^2\gamma^4\zeta^2F_0 - 15\,512\gamma^4\zeta^2F_0^3$	$a_2 = -6F^2\gamma F_0^5$
$a_{11} = 36F^4\gamma^4 + 2166F^2\gamma^4F_0^2$	$a_0 = 8\zeta^2F_0^7$

of variables A_0, γ, ζ, F, F_0, as a *jump manifold equation.* Thus, the jump manifold $\mathcal{J}\left(A_0, \gamma, \zeta, F, F_0\right)$:

$$\mathcal{J}\left(A_0; \gamma, \zeta, F, F_0\right) \;=\; \left\{\left(A_0, \gamma, \zeta, F, F_0\right): \quad J\left(A_0; \gamma, \zeta, F, F_0\right) = 0\right\}, \tag{10}$$

belongs to a $5D$ space. It is purposeful to introduce the projection of the jump manifold onto the parameter space:

$$\mathcal{J}_{\perp} \;=\; \left\{\left(\gamma, \zeta, F, F_0\right): \text{there is a real } A_0 \text{ such that } J\left(A_0; \gamma, \zeta, F, F_0\right) = 0\right\}. \tag{11}$$

In other words, for any set of parameters γ, ζ, F, F_0 belonging to $\mathcal{J}_{\perp}$, there is a jump in the dynamical system (1) and all jumps occur for the parameters belonging to $\mathcal{J}_{\perp}$.

We shall consider $2D$ and $3D$ projections, plotting $\mathcal{J}\left(A_0; \gamma_*, \zeta_*, F_*, F_0\right)$ and $\mathcal{J}\left(A_0; \gamma_*, \zeta_*, F, F_0\right)$, respectively, where the parameters γ_*, ζ_*, F_* or γ_*, ζ_* are fixed.

3.1.1 $2D$ projection, $J\left(A_0; \gamma_*, \zeta_*, F_*, F_0\right) = 0$

The global picture of the jump manifold $\mathcal{J}\left(A_0; \gamma_*, \zeta_*, F_*, F_0\right)$, where $\gamma_* = 0.0783$, $\zeta_* = 0.025$, $F_* = 0.1$ and A_0, F_0 are variable, is shown in Fig.1. We have chosen the values of γ, ζ, F such as in [1] for the sake of comparison.

All points lying on the blue curve (jump manifold) correspond to jumps (vertical tangents). Moreover, there are four critical points dividing Fig.1 into parts and referred to as the *border points*: $F_0^{(1)} = 0$, $F_0^{(2)} = 0.0920$, $F_0^{(3)} = 0.7385$, $F_0^{(4)} = 6.5321$, *where the number of jumps changes*, it is defined and computed in Subsection 3.2. More precisely, these critical points are where the red dashed vertical lines are *tangent* to the blue jump manifold.

Indeed, for $F_0 \in \left(F_0^{(1)}, F_0^{(2)}\right)$, there are two jumps; for $F_0 \in \left(F_0^{(2)}, F_0^{(3)}\right)$, there are four; for $F_0 \in \left(F_0^{(3)}, F_0^{(4)}\right)$, there are two, and there are no jumps for $F_0 > F_0^{(4)}$.

For example, in Fig.2 below, the case $F_0 = 0.4$ is shown. More exactly, the implicit function $A_1\left(\Omega\right)$, computed with the help of Eq.(7), is plotted for $\gamma = 0.0783$, $\zeta = 0.025$, $F = 0.1$, and $F_0 = 0.4$. The red dots, denoting vertical tangents, correspond to the red dots in Fig.1. These points can be easily computed from Eqs.(8), (4).

Indeed, solving equations (8) for $\gamma = 0.0783$, $\zeta = 0.025$, $F = 0.1$, $F_0 = 0.4$, we get four real solutions Ω, A_0 shown in the first two columns in Table 3. Then, for the above values of Ω, we solve equations (4) obtaining the same four values of A_0 and the corresponding values of A_1 listed in the third column of Table 3.

In Fig.3, the bifurcation diagram is shown for the set of parameters listed in Fig.2, where y is a numerical solution of Eq.(1). Note that branches a-b, c-d, e-f in Fig.3 correspond to analogous branches in Fig.2.

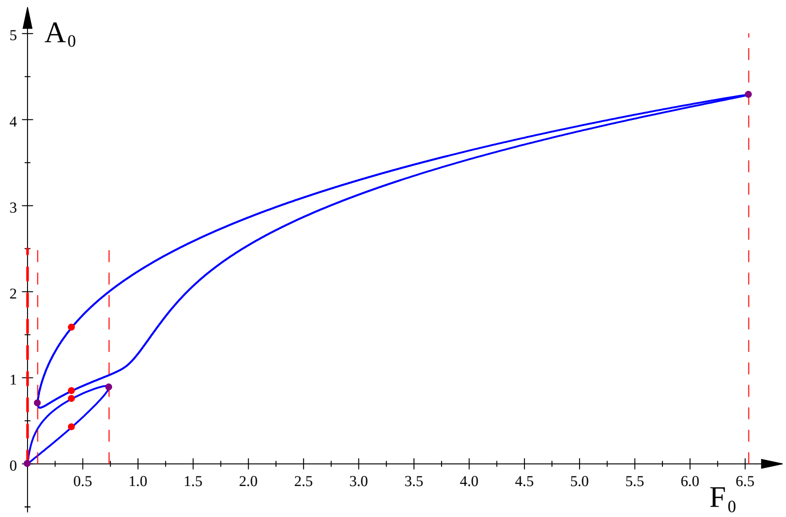

Figure 1: Jump manifold $\mathcal{J}\left(A_0;\gamma_*,\zeta_*,F_*,F_0\right)$, $\gamma_*=0.0783$, $\zeta_*=0.025$, $F_*=0.1$ (blue) and four border points (purple dots) – points of contact between $\mathcal{J}$ and the vertical red lines.

Table 3: Solutions of Eqs.(8) and (4).

Ω	A_0	A_1
0.576 122 891	0.846 633 527	1. 882 759 746
0.643 209 846	0.755 260 872	2. 032 001 367
0.690 545 624	1. 583 776 750	0.691 474 188
0.711 882 658	0.425 889 574	2. 806 379 023

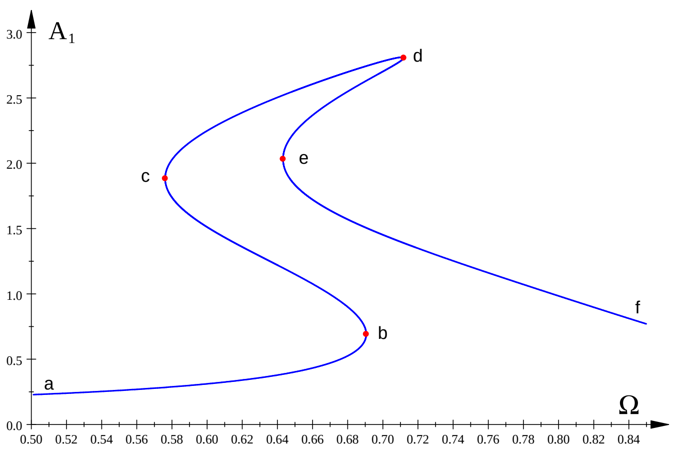

Figure 2: Amplitude-frequency response curve $A_1\left(\Omega\right)$, $\gamma=0.0783$, $\zeta=0.025$, $F=0.1$, $F_0=0.4$. Stable branches: a-b, c-d, e-f.

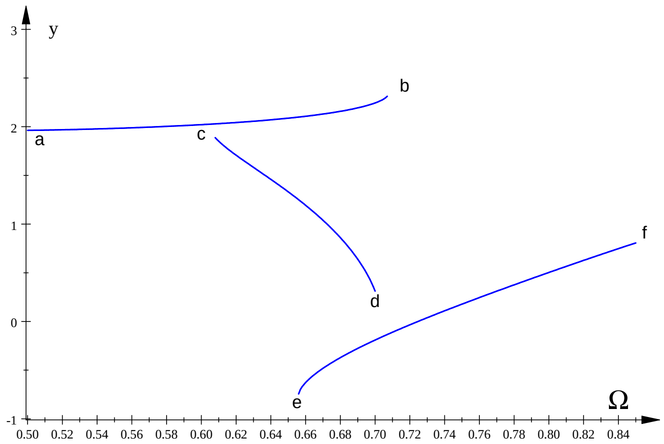

Figure 3: Bifurcation diagram, $\gamma = 0.0783$, $\zeta = 0.025$, $F = 0.1$, $F_0 = 0.4$.

3.1.2 $3D$ projection, $J(A_0; \gamma_*, \zeta_*, F, F_0) = 0$

We now fix two parameters only, for example, $\gamma_* = 0.0783$, $\delta_* = 0.025$, and plot the jump manifold $\mathcal{J}(A_0; \gamma_*, \zeta_*, F, F_0)$ as a $3D$ surface, see Fig.4.

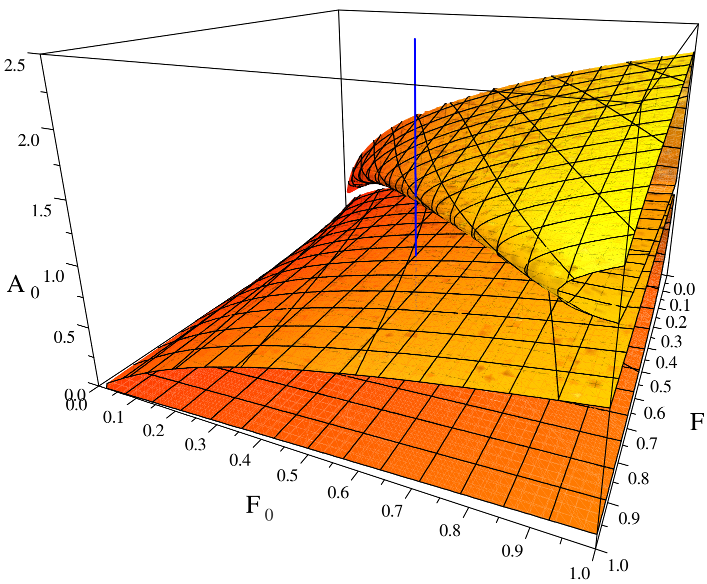

Figure 4: Jump manifold $\mathcal{J}(A_0; \gamma_*, \zeta_*, F, F_0)$, $\gamma_* = 0.0783$, $\zeta_* = 0.025$.

Next, we compute one border point. For the sake of example, we choose $F_0 = 0.5$ ($\gamma_* = 0.0783, \delta_* = 0.025$) and compute the corresponding border point as $F = 0.544\,860$, $A_0 = 1.238\,340$ as explained in the next subsection.

The blue vertical line, $(0.544\,860,\ 0.5,\ A_0)$ with A_0 variable, touches the upper lobe of the jump manifold exactly at the border point $(0.544\,860,\ 0.5,\ 1.238\,340)$.

3.2 Border sets

We shall now determine the condition for the border set: the set of points in the parameter space $(\gamma,\ \zeta,\ F_0,\ F)$ is such that the number of vertical tangents changes at these points. The mathematical condition for the border set is that the polynomial $J\left(A_0\right)$ given in Eq.(9a) and Table 2 has multiple roots.

The qualitative behavior of the polynomial equation $J\left(A_0\right)$ can be seen in Figs.1 and 4, where $2D$ and $3D$ projections of the implicit function $J\left(A_0;\gamma,\zeta,F,F_0\right)=0$ are shown. To find the parameter values for which the polynomial $J\left(A_0;\gamma,\zeta,F,F_0\right)$ has multiple roots, we demand that the resultant of $J\left(A_0\right)$ and its derivative $J'\left(A_0\right)=\frac{d}{dA_0}J\left(A_0\right)$ is zero [15]:

$$R\left(J,J';\gamma,\zeta,F,F_0\right)=0. \tag{12}$$

The resultant of the polynomial $J\left(A_0\right)$ and its derivative $J'\left(A_0\right)=\sum_{k=0}^{20}b_kA_0^k$ is a determinant of the $(m+n)\times(m+n)$ Sylvester matrix, $n=21$, $m=20$,

$$R\left(J,J';\gamma,\zeta,F,F_0\right)=\det\begin{pmatrix} a_n & a_{n-1} & a_{n-2} & \dots & 0 & 0 & 0\\ 0 & a_n & a_{n-1} & \dots & 0 & 0 & 0\\ \vdots & \vdots & \vdots & & \vdots & \vdots & \vdots\\ 0 & 0 & 0 & \dots & a_1 & a_0 & 0\\ 0 & 0 & 0 & \dots & a_2 & a_1 & a_0\\ b_m & b_{m-1} & b_{m-2} & \dots & 0 & 0 & 0\\ 0 & b_m & b_{m-1} & \dots & 0 & 0 & 0\\ \vdots & \vdots & \vdots & & \vdots & \vdots & \vdots\\ 0 & 0 & 0 & \dots & b_1 & b_0 & 0\\ 0 & 0 & 0 & \dots & b_2 & b_1 & b_0 \end{pmatrix} \tag{13}$$

and is an enormously complicated polynomial in variables $\gamma,\ \zeta,\ F,\ F_0$. However, if we fix three parameters, say $\gamma,\ \zeta,\ F$, then the equation $R\left(J,J';F_0\right)=0$ can be solved numerically and thus the critical values of F_0 can be computed.

For example, we have solved equation (12), $R\left(J,J';\gamma_*,\zeta_*,F_*,F_0\right)=0$, for $\gamma_*=0.0783$, $\zeta_*=0.025$, $F_*=0.1$, obtaining the following real positive solutions: $F_0^{(1)}=0$, $F_0^{(2)}=0.092\,075$, $F_0^{(3)}=0.738\,510$, $F_0^{(4)}=6.532\,092$. In Figs.5, the border amplitudes $A_1\left(\Omega\right)$ are shown for $\gamma=0.0783$, $\zeta=0.025$, $F=0.1$ and $F_0^{(2)}$, $F_0^{(3)}$, $F_0^{(4)}$, with critical points marked with blue crosses. At these points, jumps just appear/disappear – there is a metamorphosis of the amplitude-frequency response function. For example, the function $A_1\left(\Omega\right)$ has no jumps for $F_0>6.532\,092$, and two jumps appear for $F_0<6.532\,092$, see Fig.8.4e plotted for $F_0=0.95$ in [1]. Vertical tangents at these points are also plotted with dashed lines. Blue dots denote extant points of jumps.

We have also solved equation (12), $R\left(J,J';\gamma_*,\zeta_*,F,F_{0*}\right)=0$, for $\gamma_*=0.0783$, $\zeta_*=0.025$, $F_{0*}=0.5$, obtaining real positive solutions: $F^{(1)}=0$, $F^{(2)}=0.026\,998\,9$, $F^{(3)}=0.077\,925\,6$, $F^{(4)}=0.544\,859\,5$. Next, for $\gamma=0.0783$, $\zeta=0.025$, $F_0=0.5$, and $F=0.544\,859\,5$, we have computed from Eqs.(8) the border value $A_0=1.238\,340$, see the blue vertical line in Fig.4.

3.3 Number of solutions of Eq.(5) for a given value of Ω

There are also other qualitative changes in the amplitudes $A_1\left(\Omega\right)$ controlled by the parameters. For example, the number of solutions of Eq.(5) for a given value of Ω may

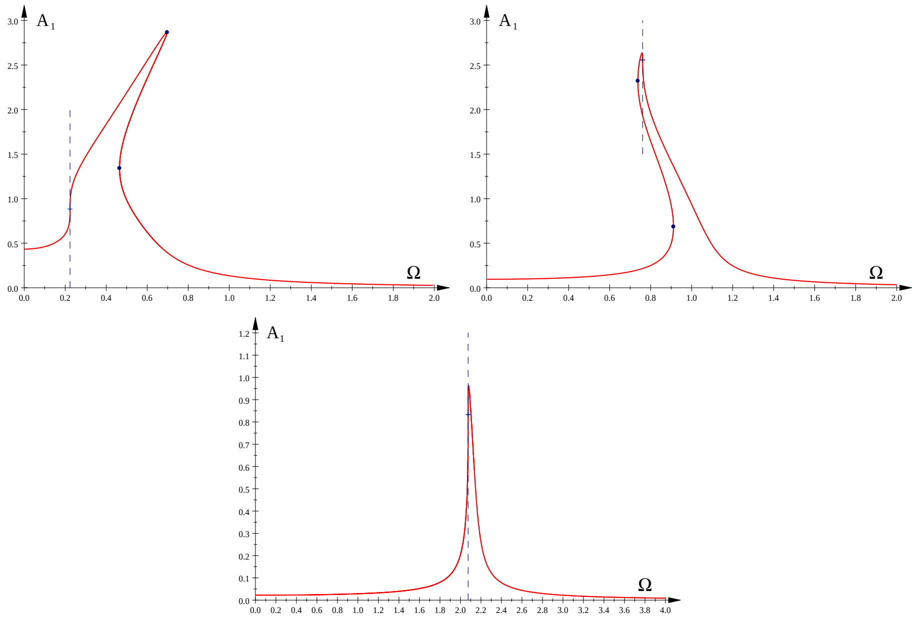

Figure 5: Amplitude-frequency response curves: $\gamma = 0.0783$, $\zeta = 0.025$, $F = 0.1$, $F_0^{(2)} = 0.092$ (top left), $F_0^{(3)} = 0.7385$ (top right), $F_0^{(4)} = 6.532$ (bottom).

change. This happens when two vertical tangents appear at the same value of Ω.

To find a value of F_0 for which this occurs, we have to find a double root Ω of equations (8). For example, let $\gamma = 0.0783$, $\zeta = 0.025$, $F = 0.1$. Now, solving Eqs.(8) numerically for several values of F_0, we easily find that for $F_0 = 0.301\,007$, there is indeed a double root: $\Omega = 0.597\,114$, $A_0 = 0.679\,284$ and $\Omega = 0.597\,114$, $A_0 = 1.\,411\,787$. There is another similar case: for $F_0 = 0.429\,166$, there is a double root: $\Omega = 0.714\,419$, $A_0 = 0.459\,118$ and $\Omega = 0.714\,419$, $A_0 = 1.\,628\,271$, see Fig.6 as well as the related Fig.9.

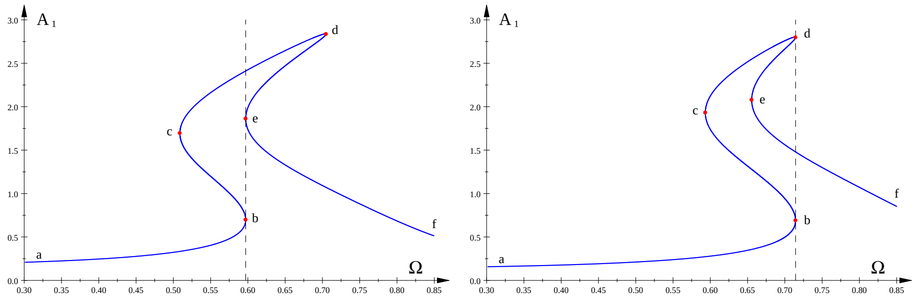

Figure 6: Amplitude-frequency response curves $A_1(\Omega)$: $\gamma = 0.0783$, $\zeta = 0.025$, $F = 0.1$, $F_0 = 0.301$ (left), $F_0 = 0.429$ (right). Stable branches: a-b, c-d, e-f.

Therefore, for $F_0 \in (0.301,\ 0.429)$, equation (5) has five solutions for some values of Ω (three stable, two unstable), see, for example, Figs.2, 3, where $F_0 = 0.4$.

4 Numerical Verification and Analysis of the Results

We start with the verification of our results for the border sets obtained in Section 3, comparing them with numerical computations carried out for the equation (1). Consider, for example, the top right figure in Fig.5. In Fig.7, we show magnification of this critical curve with a vertical tangency on the red curve and two curves: just before (green) and just after (blue) the formation of the vertical tangency.

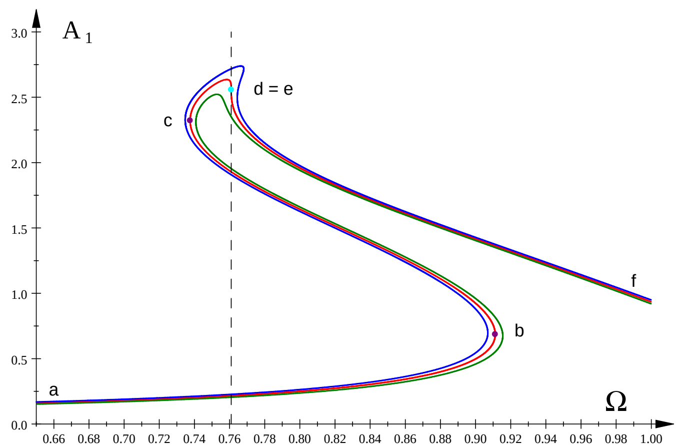

Figure 7: Implicit curves $A_1(\Omega)$: $\gamma = 0.0783$, $\zeta = 0.025$, $F_0 = 0.738\,510$ and $F = 0.095$ (green), $F = 0.1$ (red), $F = 0.105$ (blue). Critical vertical tangency on the red curve is at $(\Omega,\ A_1) = (0.761,\ 2.558)$ (light blue-green dot).

Recall that we have solved equation (12) for $\gamma = 0.0783$, $\zeta = 0.025$, $F = 0.1$, obtaining four real positive solutions: $F_0^{(1)} = 0$, $F_0^{(2)} = 0.092\,075$, $F_0^{(3)} = 0.738\,510$, $F_0^{(4)} = 6.532\,092$. Curves in Fig.7 have been plotted for $\gamma = 0.0783$, $\zeta = 0.025$, $F_0^{(3)} = 0.738\,510$ and $F = 0.095$ (green), $F = 0.1$ (red), $F = 0.105$ (blue). We have decided to plot curves $A_1(\Omega)$ for the variable F since the shapes of these curves are very sensitive to this parameter.

When we pass from the green to the red curve, we note the formation of vertical tangency on the red curve. Stable branches on the red curve are: a-b, c-d=e, and d=e-f.

In Fig.8, we show the bifurcation diagrams computed by solving numerically Eq.(1) for the values of the parameters γ, ζ, F_0 such as in Fig.7 and $F = 0.114$ (green), $F = 0.116$ (blue), respectively.

These two bifurcation diagrams correspond qualitatively to the green and blue curves $A_1(\Omega)$ in Fig.7. The main difference between these two plots is a discontinuity of the blue curve corresponding to the creation of the jump phenomenon at $\Omega = 0.785$.

Note that the discontinuity appears in the interval $F \in (0.114,\ 0.116)$ while the analytically predicted value is $F = 0.1$. This discrepancy can be attributed to the error of the asymptotic method used to compute the solution (2a).

We now discuss the results obtained in Subsection 3.3. In Fig.9, two bifurcation diagrams are shown, corresponding to the amplitude-frequency curves shown in Fig.6. Two Figures 6 were computed for $\gamma = 0.0783$, $\zeta = 0.025$, $F = 0.1$ and $F_0 = 0.301$ and $F_0 = 0.429$ can be set together with Figures 8.4b, 8.4c, 8.4d from Ref. [1], computed

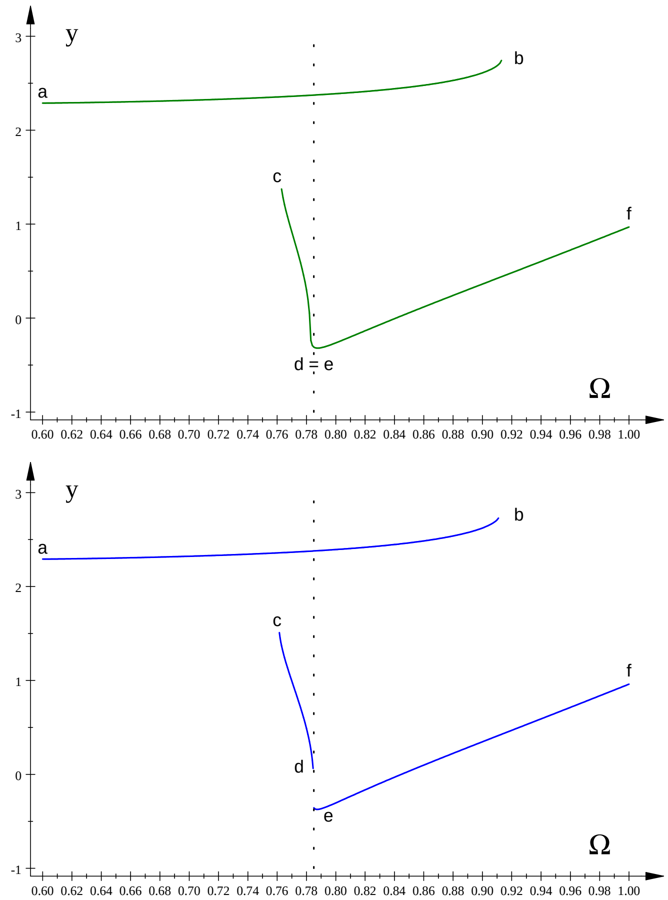

Figure 8: Bifurcation diagrams: $F = 0.114$ (green), $F = 0.116$ (blue), the values of the parameters γ, ζ, F_0 are the same as in Fig.7. Discontinuity is at $\Omega = 0.785$.

for the same values of γ, ζ, F and for $F_0 = 0.2$, $F_0 = 0.4$, $F_0 = 0.5$, respectively. The sequence of the amplitude-frequency curves plotted for $F_0 = 0.2,\ 0.301,\ 0.4,\ 0.429,\ 0.5$ shows the metamorphoses of these curves.

In Figures 6, there are two different jumps for the same value of Ω. Indeed, in the bifurcation diagrams shown in Fig.9, two different branches of the solution of Eq.(1) end or begin at the same value of Ω (these places are denoted in Fig.6 and Fig.9 as "b" and "e").

It follows that three stable solutions of Eq.(1) are in the interval $F_0 \in (0.284,\ 0.395)$, $\gamma = 0.0783$, $\zeta = 0.025$, $F = 0.1$, while analytical prediction was $F_0 \in (0.301,\ 0.429)$ (see the end of Subsection 3.3). This discrepancy is again due to the unavoidable errors of the asymptotic method.

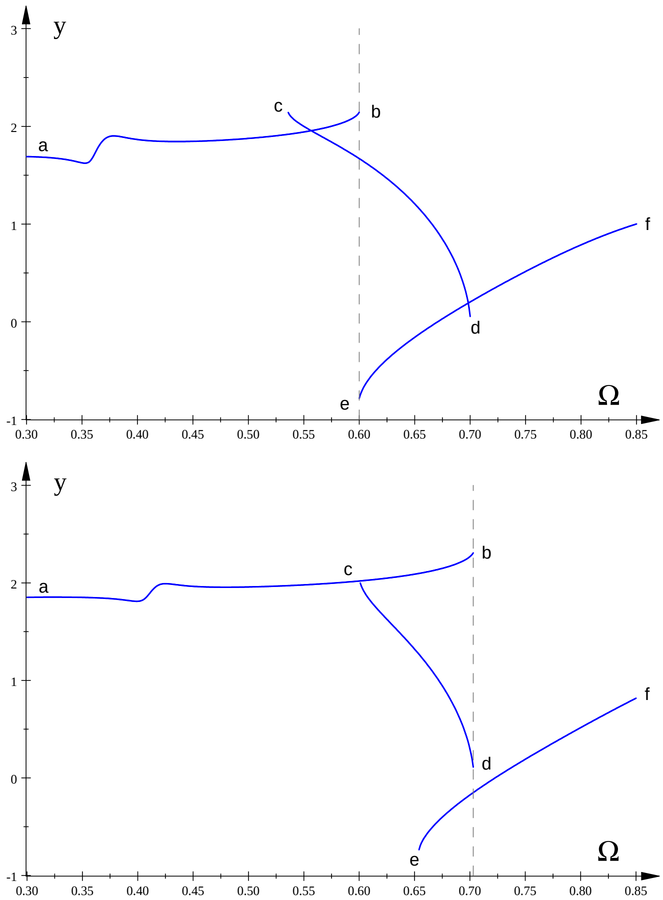

Figure 9: Bifurcation diagrams: $\gamma = 0.0783$, $\zeta = 0.025$, $F = 0.1$, $F_0 = 0.284$ (top), $F_0 = 0.395$ (bottom).

5 Summary

Working in the implicit function framework [10], we have computed the jump manifold, cf. (10) and Table 2, including information about all jumps in the dynamical system (1).

Our work on the asymmetric Duffing oscillator is a supplementation and amplification of the results obtained by Kovacic and Brennan [1]. The sequence of Figures 8.4 (a) –(e), computed in [1] for $\gamma = 0.0783$, $\zeta = 0.025$, $F = 0.1$, and $F_0 = 0.01$, 0.2, 0.4, 0.5, 0.95, respectively, can be appended with Figs.5 and 6 computed for $F_0 = 0.092$, 0.7385, 6.532, and $F_0 = 0.301$, 0.429. The sequence of metamorphoses of the curve $A_1(\Omega)$ consists of the plots computed for $F_0 = \mathbf{0.01}$, 0.092, $\mathbf{0.2}$, 0.301, $\mathbf{0.4}$, 0.429, $\mathbf{0.5}$, 0.7385, $\mathbf{0.95}$, 6.532, where the numbers highlighted in bold correspond to Figs.8.4 (a)–(e) plotted in [1].

We show in Section 4 how a jump phenomenon arises in the dynamical system (1) and how it can be predicted based on a solution of Eq.(3), see Figs.7, 8. In short, the dynamical signature of the appearance of the jump phenomenon consists in a rupture of a stable branch, see Fig.8. Jumps are created at a border set, see Eqs.(12), (13). We have computed the values of parameter F_0, at which a change of multi-stability occurs.

References

[1] I. Kovacic and M.J. Brennan. Forced harmonic vibration of an asymmetric Duffing oscillator. In: *The Duffing Equation: Nonlinear Oscillators and Their Behavior.* (Eds.: I. Kovacic, M.J. Brennan). John Wiley & Sons, Hoboken, New Jersey 2011, pp. 277–322.

[2] I. Kovacic, M.J. Brennan (Eds.). *The Duffing Equation: Nonlinear Oscillators and Their Behavior.* John Wiley & Sons, Hoboken, New Jersey 2011.

[3] Y. Ueda. Explosions of strange attractors exhibited by Duffing equation. *Ann. N.Y. Acad. Sci.* **357** (1980) 422–433.

[4] Y. Ueda. Randomly transitional phenomena in the systems governed by Duffing's equation. *J. Stat. Phys.* **20** (1979) 181–196.

[5] W. Szemplińska-Stupnicka and J. Bajkowski. The 1/2 subharmonic resonance and its transition to chaotic motion in a non-linear oscillator. *Int. J. Non-Linear Mech.* **21** (1986) 401–419.

[6] T. Kalmár-Nagy and B. Balachandran. Forced harmonic vibration of a Duffing oscillator with linear viscous damping. In: *The Duffing Equation: Nonlinear Oscillators and Their Behavior).* (Eds.: I. Kovacic, M.J. Brennan). John Wiley & Sons, Hoboken, New Jersey 2011, pp. 139 – 174.

[7] A.H. Nayfeh. *Introduction to Perturbation Techniques*, John Wiley & Sons, 2011.

[8] M. Wali Ullah, M. Alhaz Uddin and M. Saifur Rahman. A Modified Harmonic Balance Method for Solving Strongly Generalized Nonlinear Damped Forced Vibration Systems, *Nonlinear Dyn. Syst. Theory* **21** (2021) 544–552.

[9] D.W. Jordan and P. Smith. *Nonlinear Ordinary Differential Equations*, Oxford University Press, New York, 1999.

[10] J. Kyzioł and A. Okniński. Localizing bifurcations in nonlinear dynamical systems via analytical and numerical methods, *Processes* **10** (2022) 127, 17 pages.

[11] Q. Bi. Dynamical analysis of two coupled parametrically excited van der Pol oscillators, *Int. J. Nonlinear Mech.* **39** (2004) 33–54.

[12] Akram Khalil Cheib, V.E. Puzyrov and N.V. Savchenko. Analysis of the Dynamics of a Two-Degree-of-Freedom Nonlinear Mechanical System under Harmonic Excitation, *Nonlinear Dyn. Syst. Theory* **20** (2020) 168–178.

[13] J. Kyzioł, A. Okniński. Metamorphoses of resonance curves in systems of coupled oscillators: The case of degenerate singular points, *Int. J. Non-Linear Mech.* **95** (2017) 272–276.

[14] C.T.C. Wall. *Singular Points of Plane Curves*, Cambridge University Press, New York 2004.

[15] S. Janson. Resultant and discriminant of polynomials, Lecture notes, 2010. Available at `http://www2.math.uu.se/~svante/papers/sjN5.pdf`.